CrossMark

RESEARCH PAPER

Synthesis of CdS-decorated RGO nanocomposites by reflux condensation method and its improved photocatalytic activity

Nannan Meng · Yifeng Zhou · Wangyan Nie · Pengpeng Chen

Abstract The cadmium sulfide nanoparticle-reduced graphene oxide (CdS/RGO) nanocomposite with intimate nano-interfacial contact was successfully prepared via a facile condensation process in dilute dimethylformamide (DMF) aqueous solution. Numerous CdS nanoparticles featuring a size of around 10 nm were homogeneously anchored on 2D nanosheets. During the formation of CdS/RGO nanocomposite, graphene oxide (GO) was transformed into RGO simultaneously. The solar-driven degradation of Rhodamine B (RhB) was conducted to detect the activity of the as-prepared CdS/RGO nanocomposite. Significantly, the photocatalytic activity of CdS/RGO nanocomposite was almost three times higher than that of pure CdS. The charge transfer and photogenerated active hydroxyl radicals ($\cdot$OH) were investigated to study the mechanism of excellent photocatalytic property. The synthetic method provided a valuable opportunity to fabricate large-scale novel graphene-based materials with superior catalytic activity.

Keywords CdS/RGO nanocomposite · Reflux condensation method · Photocatalysis · Photochemical catalysis mechanism · Mitigate environmental pollution

N. Meng · Y. Zhou · W. Nie · P. Chen (✉)
Anhui Province Key Laboratory of Environment-Friendly Polymer Materials, School of Chemistry & Chemical Engineering, Anhui University, No. 111, Jiulong Road, Hefei 230601, Anhui, People's Republic of China
e-mail: chenpp@ahu.edu.cn

Introduction

In recent years, a great deal of effort has been contributed to eliminating pollution of effluents from urban and agricultural industries with organic pollutants (Li et al. 2015a; Ajmal et al. 2014; Konstantinou and Albanis 2004). Photocatalysis has caused an increasing attention because of its widespread environmental applications such as water disinfection, CO_2 reduction and air cleanup (Yin et al. 2014; Paramasivam et al. 2012). Among various photocatalysts, CdS has attracted great attention because of its optimal band gap (about 2.4 eV) for effective absorption of sunlight leading to easily transform solar energy into chemical energy under solar light irradiation (Han et al. 2015). However, due to the fact that the rapid recombination rate of photogenerated charge carriers leads to low energy-transfer efficiency, investigations and applications of neat CdS have been greatly limited (Zhang et al. 2013a). Since the photocatalytic nanocomposites with multiple kinds of functional ingredients can exert the advantages of different ingredients to conquer the shortages of neat ingredient photocatalyst, the various types of heterogeneous photocatalysts have been explored for enhanced photocatalysts by dominantly increasing the light absorption and/or improving the charge separation and transportation via constructing heterostructures (Qu and Duan 2013).

Recently, with high chemical stability, notably high specific surface area and superior conductivity,

graphene has received extensive attention in almost every field of engineering and science (Singh et al. 2011). As those intriguing characters, graphene provides an exciting opportunity to yield highly efficient photocatalysts. Nanocomposites of CdS and graphene have presented noteworthy advantageous enhancement of photocatalytic performance in a number of works dominatingly because the graphene can work as a charge carrier transporter in photocatalytic system. Li et al. (2011) revealed that CdS/RGO nanocomposite exhibited a high activity in the photocatalytic production of H_2 from water splitting. Yu et al. (2014) applied CdS/RGO nanocomposite to the photocatalytic CO_2 reduction and excellent reduction efficiency of CO_2 to CH_4 was discovered. Liu et al. (2014) demonstrated the photocatalytic activity of CdS/RGO nanocomposite for dye degradation was obviously higher than that of pure CdS. Excellent CdS/graphene photocatalysts are also applicable to reduce Cr(VI) into Cr(III) (Liu et al. 2011), photocatalytic antibacterial (Gao et al. 2013) and controllable organic photosynthesis (Zhang et al. 2013c). Besides its various photocatalytic applications, CdS/RGO nanocomposites are also valued in many other categories such as biosensors (Li et al. 2015b), solar cells (Yuan et al. 2014), photovoltaic devices (Yan et al. 2012) and so on.

As for its wide application outlook and much great value in engineering, the preparation of CdS/graphene nanocomposite is full of significance and vital importance. So far, numerous synthetic techniques have been adapted to fabricate CdS/RGO nanocomposite. For example, CdS nanoparticles were anchored on RGO by layer-by-layer (LBL) self-assembly fabrication technology (Xiao et al. 2014), solvothermal method (Liu et al. 2013) and microwave-assisted method (Liu et al. 2011). In addition, CdS/RGO hybrids could be synthesized via reducing GO with various reductants, such as hydrazine (Cao et al. 2010) and H_2S (Nethravathi et al. 2009). Those approaches were demonstrated to be efficient for the fabrication of CdS/RGO nanocomposite and enhancement of CdS catalytic abilities, but toxic reagents, expensive apparatus or dangerous and complicated operations are always involved, which greatly restricts their broad application in reality. Therefore, it is necessary to search a convenient approach for the preparation of CdS/RGO nanocomposite.

Here, we report a reflux condensation method in water–DMF mixed solution for the synthesis of CdS/RGO nanocomposite (shown as Scheme 1), which is a facile approach operated with the advantages of low cost and simplicity. Such a method avoids using toxic reduction reagents such as hydrazine and complex chemical procedure. Importantly, the utilization of the DMF reagent as reducing agent is very promising because it is inexpensive and abundant in chemical industries (Ai et al. 2011). Most importantly, the as-obtained CdS/RGO nanocomposite shows excellent photocatalytic performance.

Experimental section

All raw materials were analytical grade and used as purchased without further purification.

Preparation of CdS

An equimolar amount of $Na_2S \cdot 9H_2O$ solution was added to a solution of $Cd(CH_3COO)_2 \cdot 2H_2O$ with stirring for 2 h at room temperature. The product was recovered by filtration, rinsed three times with deionized water, and finally dried at 80 °C under vacuum.

Preparation of CdS/RGO nanocomposite

Graphene oxide (GO) was synthesized from natural graphite in accordance with our recently reported method (Liu et al. 2015; Meng et al. 2015a). CdS/RGO was fabricated by reflux condensation method under atmospheric pressure. In a typical procedure, 10 mg of GO and 0.2 g of CdS were well dispersed in 60 mL of the water–DMF mixed solution (volume ratio: $DMF/H_2O = 2/1$) by sonication. Next, the reaction system was constantly stirred using a magnetic stirrer at 115 °C in oil bath for 10 h. Finally, the product was washed three times with distilled water and ethyl alcohol by centrifugation and dried at 80 °C under vacuum over a night. To investigate the optimum ratio between them, a series of similar syntheses with different weight ratio of GO to CdS (weight ratio: 2.5, 5.0 and 10.0 %, marked as CG-1, CG-2 and CG-3, respectively.) was carried out. Additionally, a physical mixture of GO and CdS (weight ratio 5.0 %) was also fabricated for comparison via mechanical blending method using an agate mortar.
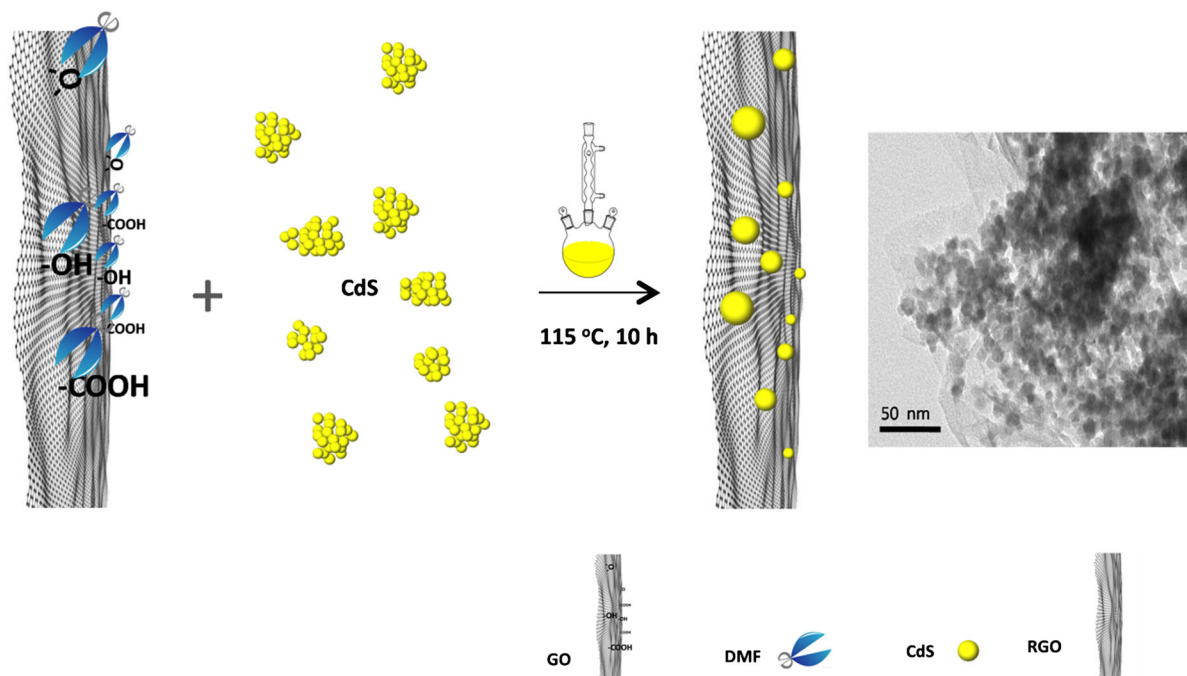
Scheme 1 The preparation of CdS/RGO nanocomposite

Characterizations

XRD patterns of the samples were obtained with a PERSEE XD-3 diffractometer (Cu Kα, $\lambda = 0.154178$ nm, scanning rate of 4°/min, step scan of 0.02°, 36 kV, 20 mA). The dispersion of sample was measured using a UV-1800 spectrophotometer (SHIMADZU). The morphology of sample was observed using TEM (JEM-2100, Hitachi, 200 kV). DRS of the samples were measured in the ultraviolet–visible region using a U-4100 spectrophotometer with an integrating sphere (Hitachi, $BaSO_4$ as a reference). FT-IR spectra were collected on a Nexus 870 spectrometer (Nicolet). The Raman profile of sample was recorded on an inVia-Reflex (Renishaw 532 nm). Fluorescence spectrum (FL) was characterized by an F-7000 spectrophotometer (Hitachi). XPS was performed by a VG Microtech ESCA2000 (Al Kα X-ray source, 1486.6 eV). Nyquist plots of EIS were collected in 0.1 M phosphate buffer (pH = 7.4) solution containing 0.1 M KCl and 5 mM $Fe(CN)_6^{4-/3-}$ using an IM6 (Zahner, three-electrode system: a Pt counter electrode, an Ag/AgCl reference electrode and a GCE work electrode.).

Photocatalytic activity

The photocatalytic performance of the samples was evaluated by photocatalytic degradation of RhB aqueous solution under solar light illumination simulated with a Xe lamp (300 W HSX-F300 lamp, Beijing Nbet Technology Co., Ltd.). The distance between lamp and photocatalytic reactor was 15 cm. 8 mg of the sample was dispersed in 50 mL of the RhB (10 ppm). Prior to irradiation, the suspension was agitated for 30 min in the dark on a magnetic stirrer at room temperature to reach an adsorption–desorption balance between the sample and reactant. For 60-min irradiation, 4 mL of sample dispersion was collected before and after every 10 min of illumination and the photocatalyst was completely removed by centrifugation at 10,000 rpm for 6 min. Subsequently, the supernate was determined by monitoring the absorption peak at 554 nm using UV–Vis absorption spectrophotometer. Methyl blue (MB), and Methyl orange (MO) were also analyzed under the same conditions and monitored its absorption peak at 664 and 464 nm, respectively. Photogenerated active radical ·OH was detected by PL spectrum using terephthalic acid (TA)

as a probe molecule. The procedure were performed as the aforementioned measurement of photocatalytic activity and the difference was that the dye aqueous solution was exchanged by 50 mL of NaOH $(2 \times 10^{-3}$ M) and TA $(5 \times 10^{-4}$ M).

Calculation

Based on the Beer–Lambert's law (Meng et al. 2015b), the intensity of the character absorption peak of RhB at 554 nm was linearly proportional to its concentration. Therefore, the photodecomposition efficiency of RhB could be calculated using the following equation [degradation rate (Dr) or residual rate (Rr) %]:

$$Dr \% = 100 \% - Rr \%$$

$$Rr \% = (C_t/C_0) \times 100 \%$$

where Dr % or Rr % reflects photocatalytic activity, C_0 and C_t are corresponding to absorbances after absorption–desorption equilibration and t min irradiation, respectively. The pseudo-first-order reaction was adopted to calculate the photocatalytic reaction kinetics using the following equation (Wu et al. 2015):

$$\ln(C_t/C_0) = -Kt$$

where K is apparent rate constant.

Results and discussion

Figure 1a displays the XRD profiles of the native graphite and GO samples. In Fig. 1a, the XRD pattern of GO showed a relatively weak peak at $2\theta = 10.9^{\circ}$, with d-spacing of 0.81 nm, which was much larger than 0.34 nm of natural graphite at $2\theta = 26.5^{\circ}$. This change confirmed that natural graphite had already successfully oxidized to GO (Etmimi and Sanderson 2011). Peaks at 230 and 300 nm in UV–Vis absorption spectrum of GO (the insert) were caused by π–π^* transition of the C=C band and n–π^* transition of C=O band (Shown et al. 2014), respectively. Figure 1b displays the XRD spectra of the CdS and CdS/RGO nanocomposites. For the CdS, only three weak and broad diffraction peaks at 26.5°, 44.0°, and 52.0°, were observed, which were indexed to the (111), (220), and (311) planes of zinc blende crystal CdS structure

(ICDD card No. 65-2887), suggesting the small sizes and poor crystallinity of CdS nanoparticles (Veamatahau et al. 2015). However, any diffraction peaks of RGO could not be observed in all the present XRD patterns of CdS/RGO nanocomposites with different RGO contents. It was due to the well exfoliation of layer-stacking regularity of graphite, low diffraction intensity (Liu et al. 2013).

The structure information was further investigated by FT-IR spectrum and Raman technique. Figure 2a shows FT-IR spectra of the synthesized GO and CdS/RGO nanocomposite. The FT-IR peaks of GO corresponding to the oxygenic groups including the C=O (1726 cm^{-1}), O–H (1410 cm^{-1}), C–O (epoxy; $1250 \text{ cm}^{-1})$, C–O (alkoxy; $1077 \text{ cm}^{-1})$ and C=C (1625 cm^{-1}) were observed (Zhang et al. 2010). Compared with the absorption peaks of the oxygen functionalities in GO, the intensity of those absorption peaks in the CdS/RGO nanocomposite was significantly decreased, and absorption peaks of C–O (epoxy) and C=O corresponding to 1250 and 1726 cm^{-1} were nearly absent, meaning GO reduction and the formation of graphene occurred during the reflux treating process. A broad peak around 644 cm^{-1} that appeared in CdS/RGO profile could be attributed to the Cd–S bond (Ge et al. 2012). Figure 2b displays the typical Raman spectra of GO, CdS and as-prepared CdS/RGO hybrid structure. In Fig. 2b, two well-identified GO Raman peaks could be observed at 1345 and 1590 cm^{-1}, which were attributed to the D band and G band, respectively. Both of them were also presented in the Raman spectrum of CdS/RGO nanocomposite. However, the intensity ratio of D to G increased remarkably compared with that of GO, indicating the formation of RGO in CdS/RGO hybrid (Song et al. 2012). The Raman peaks at 300, 600 and 900 cm^{-1} in CdS/RGO nanocomposite were, respectively, assigned to the first-order (1LO), second-order (2LO), and third-order longitudinal optical phonon modes (3LO) of CdS (Kaveri et al. 2013). Compared with the intensity ratio of 2LO to 1LO (2LO/1LO) of CdS, the strength of electron-vibration coupling was a noteworthy increase from 0.34 to 0.43 after it was closely coupled with RGO. This increment of the 2LO/1LO ratio suggested the strong interaction between CdS nanoparticles and RGO, which devoted to enhancement of its photochemical properties (Bera et al. 2015).

TEM and HR-TEM images were employed to directly observe the microscopic morphology and
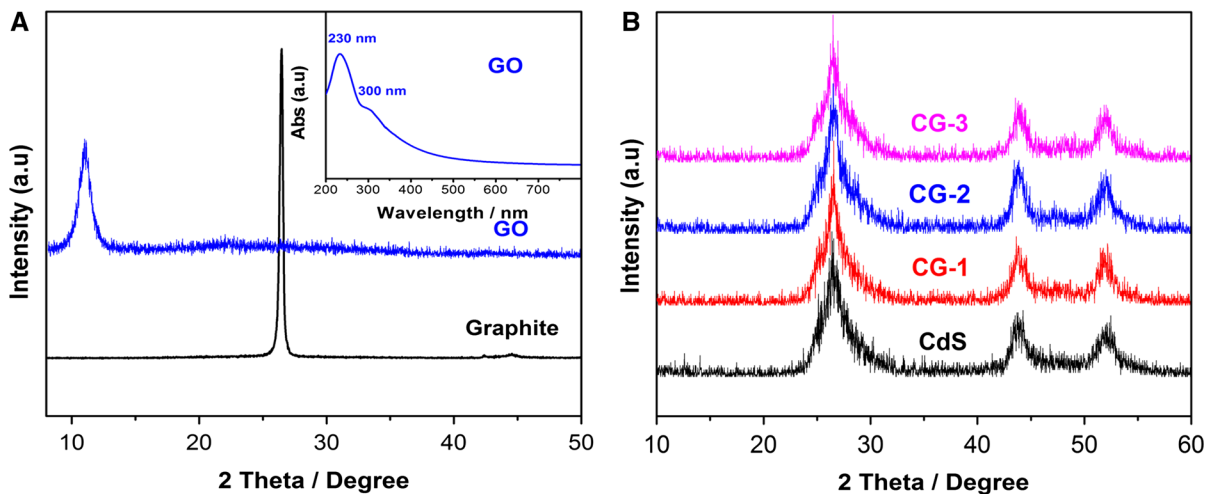
Fig. 1 **a** XRD patterns of graphite and GO (Inset: UV–Vis of GO); **b** XRD patterns of CdS and CdS/RGO nanocomposites with different RGO contents
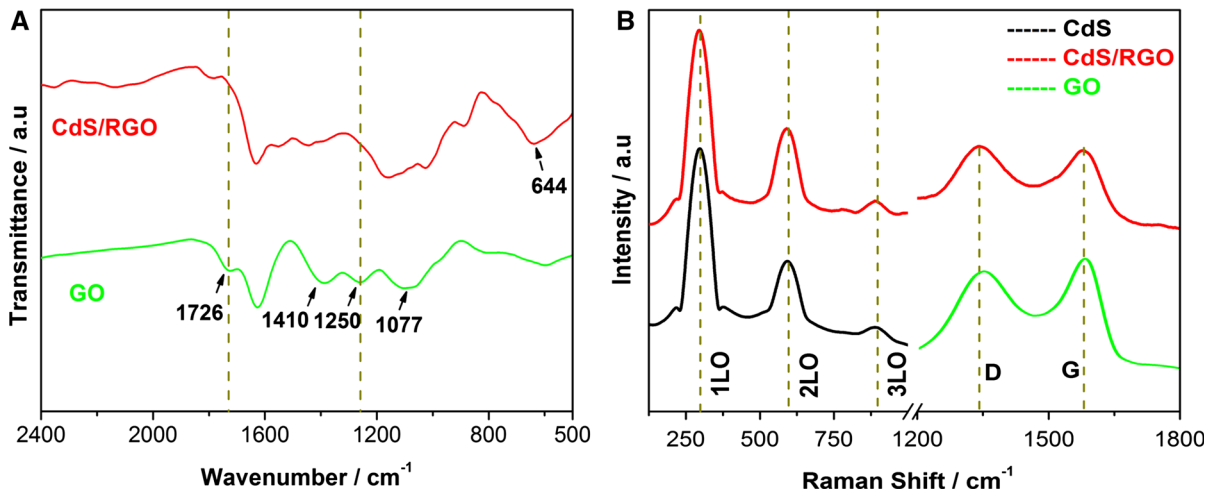

Fig. 2 **a** FT-IR profiles of GO and CdS/RGO; **b** Raman spectra of GO, CdS nanoparticles and CdS/RGO nanocomposite

structure information of the GO and CdS/RGO as shown in Fig. 3. Figure 3a shows a general view of the bare GO nanosheets, indicating that the exfoliated GO sheets were very clean and had a smooth surface. Figure 3b shows the neat CdS nanoparticles presented serious self-aggregation. After compositing with RGO (Fig. 3c, d), numerous CdS nanoparicles were homogenously and tightly coated on the layered RGO, even after preceding a long time intensive ultrasonic process. The numerous CdS nanoparticles were homogenously coated on the layered RGO featuring intimate nano-interfacial contact which would bring advantage for the charge transfer process

between them, thereby devoting to the improvement of photoactivity. From the HR-TEM image (Fig. 3e), the lattice fringe with interplanar spacing of 0.336 nm was well resolved, which could be assigned to the (111) plane of the RGO-supported CdS nanoparticles (Ge et al. 2012). The corresponding selected area electron diffraction (SAED) pattern (Fig. 3f) was consistent with zinc blende crystal CdS structure (Veamatahau et al. 2015).

The reduction of GO in CdS/RGO nanocomposite was further investigated by XPS instrument. Figure 4a, b shows the high-resolution curves of C 1 s peak of GO and CdS/RGO. The spectrum of Fig. 4a
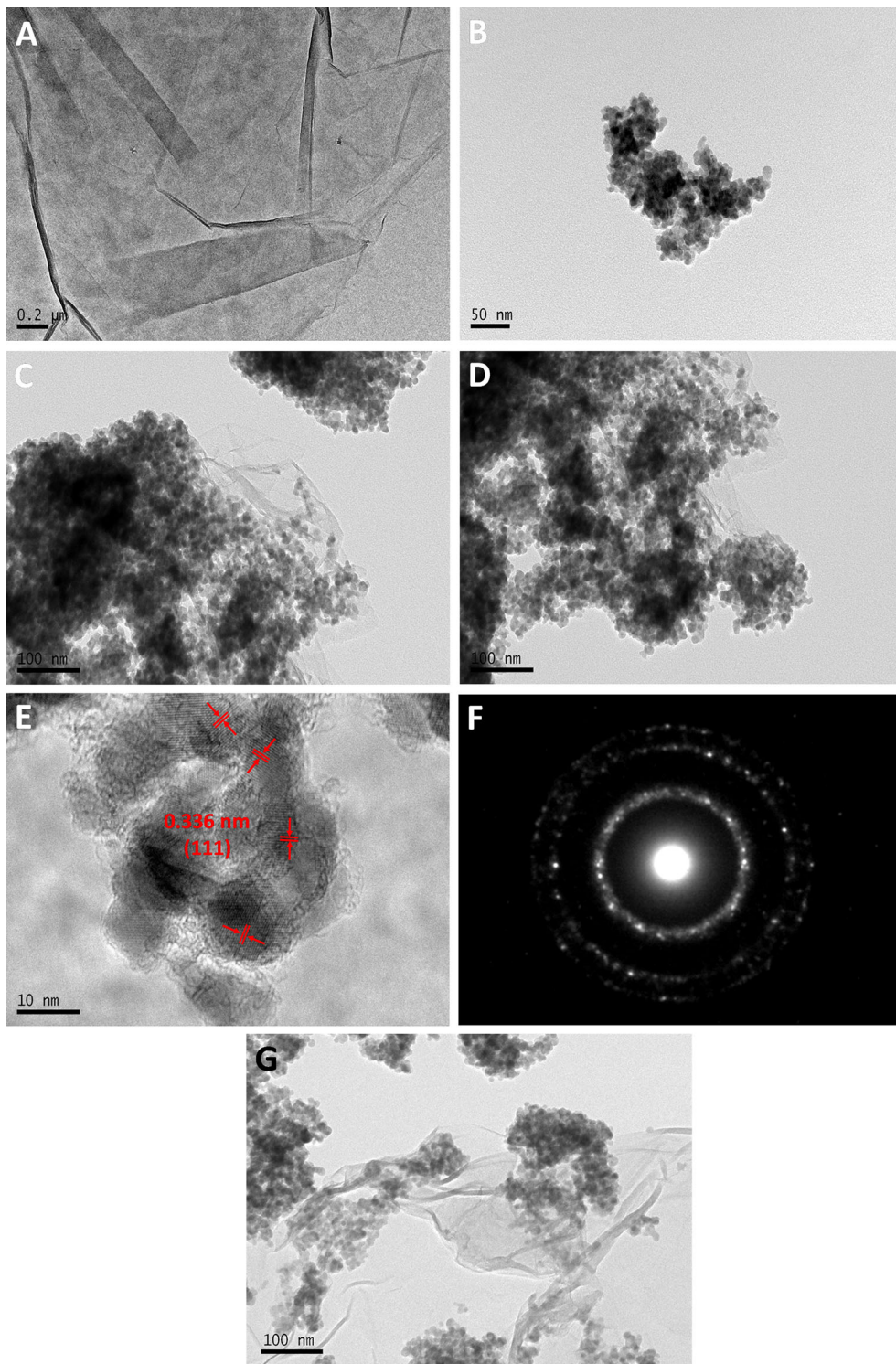
Fig. 3 **a** TEM images of GO, **b** neat CdS and **c**, **d** CdS/RGO nanocomposite; **e** HR-TEM and **f** SAED of CdS/RGO nanocomposite; **g** TEM image of the physical mixture of GO and CdS

could be fitted into three main components arising from hydroxyl and epoxy (C–O, 286.5 eV), C–C/C=C in aromatic rings (284.5 eV) and carbonyl (C=O, 288.5 eV) groups (Zhang et al. 2011), respectively. However, after formation of the CdS/RGO nanocomposite, the peak intensity of these oxygenic groups was significantly decreased (Fig. 4b), especially for C–O and carbonyl groups, which indicated the reduction by DMF during the condensation process. The binding energies 405.0 and 411.7 eV in Fig. 4c were attributed to the binding energies of the Cd $3p_{5/2}$ and $3p_{3/2}$ electrons (Chen et al. 2015a). The XPS peaks at 161.9 and 163.1 eV aroused from S 2p signals (Fig. 4d) (Chen et al. 2015b). The XPS spectra further demonstrated the conclusion that CdS had already been effectively coupled with RGO nanosheets.

Both light absorption threshold and band gap energy of samples were detected by DRS technique. Figure 5a presents the plots of absorbance vs. wavelength for CdS and CdS/RGO. Compared with the absorption spectrum of CdS, the spectrum of CdS/RGO nanocomposite exhibited stronger absorption over the whole UV–Vis region, indicating its higher solar light harvesting efficiency. Additionally, the band gap (E_g) of the samples had been further calculated using following equation (Park et al. 2015; Deng et al. 2014):

$$[\alpha h\upsilon]^n = k(h\upsilon - E_g)$$

where $h\upsilon$ is the discrete photon energy; α is the absorption coefficient; k is a constant; n is equal to 2 (the allowed direct transitions); E_g is the band gap. The
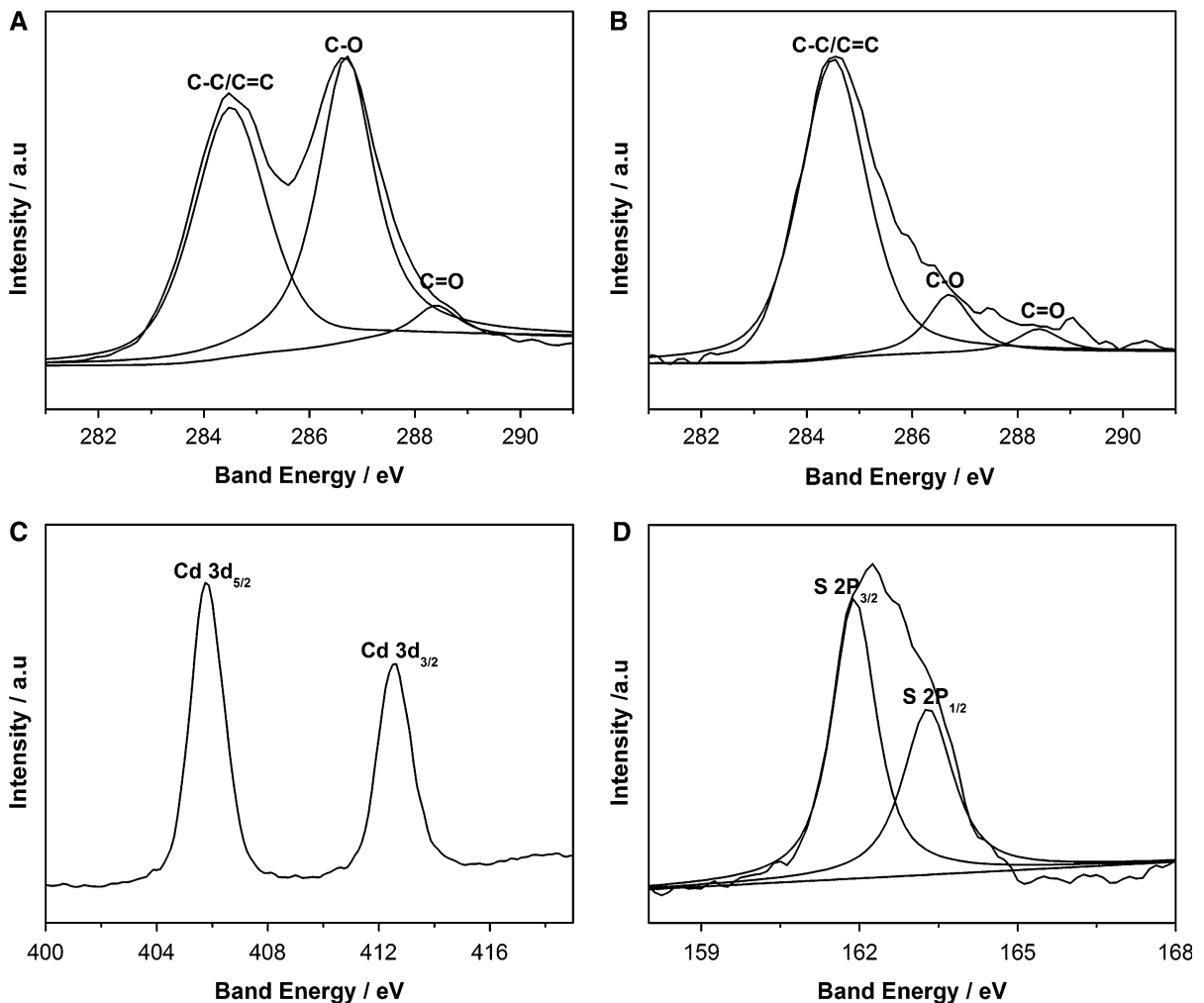
Fig. 4 XPS spectra of GO (**a**) and CdS/RGO nanocomposite (**b, c, d**): **a** C 1 s, **b** C 1 s, **c** Cd 3d, **d** S 2p
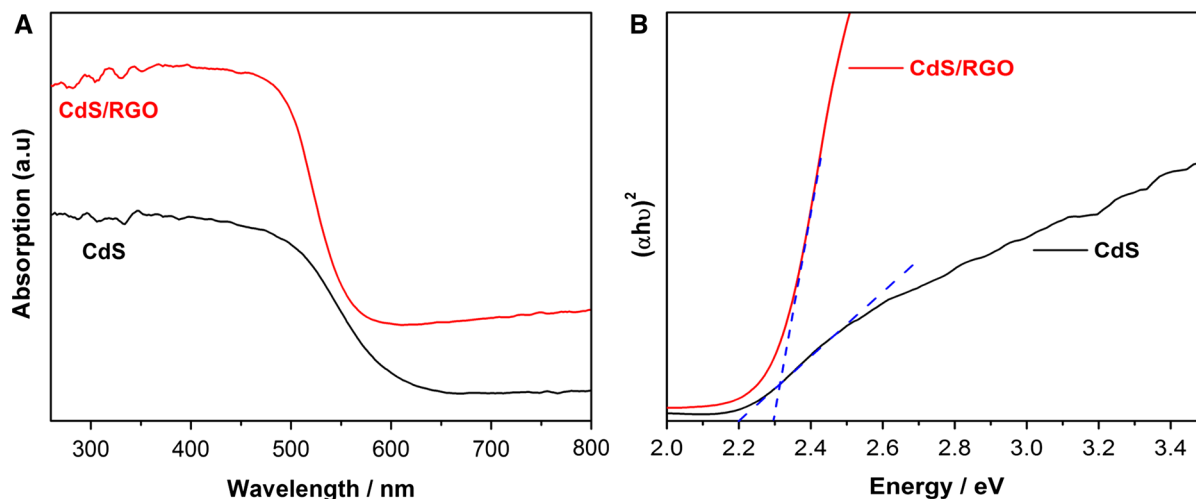
Fig. 5 **a** DRS of CdS and CdS/RGO nanocomposite; **b** [αhυ]^2 vs. hυ curve of CdS and CdS/RGO nanocomposite

band gap plots of [αhυ]^2 vs. hυ are presented in Fig. 5b. The calculated band gaps were 2.20 and 2.29 eV for CdS and CdS/RGO nanocomposites, respectively. Compared to the band gap of CdS, the blue shift of CdS/RGO nanocomposite was attributed to the internal stress induced by structural defects (Park et al. 2015), which was aroused by reflux treating process.

To evaluate the photocatalytic activity of the nanocomposite and confirm the efficiency of construction approach, the photocatalytic ability of CdS/RGO was then examined by decomposition of organic pollutant under solar irradiation. Figure 6a shows the contrast photocatalytic performance between CdS and CdS/RGO with different RGO contents and the photocatalytic RhB degradation reaction was monitored through its characteristic absorption peak at 554 nm. In the light of photoactivity data, it was clear to see that the all of CdS/RGO nanocomposites exhibited significantly improved photocatalytic ability as compared to CdS. The amount of RGO in the nanocomposites was an important factor affecting decomposition activity. With the increasing RGO content in the nanocomposites, the RhB degradation rate was initially increased and then decreased. The optimum content of RGO to CdS was 5 %, which CdS/RGO sample showed the best activity in degradation of RhB. The controlled experiment for comparison of catalytic activities between CG-2 and a physical mixture of GO and CdS (weight ratio of GO to CdS

was the same as CG-2) was performed. As we could see from Fig. 6a, the degradation rate of physical mixture was much lower than CG-2. Observed from the TEM image of the physical mixture of GO and CdS (Fig. 3g), physical mixture presented distinct phase separation and low loading of CdS nanoparticles, suggesting its poor interface interaction, simultaneously, the abundant oxygen-containing groups of GO with inferior conductivity also devoted to its weak photocatalytic performance (Zhao et al. 2012; Bera et al. 2015; Guo et al. 2015). These results demonstrated that CdS/RGO nanocomposite possessed excellent photocatalytic activity in RhB decomposition and the effective reflux construction method. CG-2 was further used to degrade other organic dyes, MB and MO, under the same conditions and the results are displayed in Fig. 6b. After illumination for 30 min, the Rr % of MO, MB and RhB were 64.3, 23.7 and 1.4 %, respectively. The apparent rate constants were calculated to be 9.2×10^{-2}, 6.2×10^{-2} and 1.7×10^{-2} min^{-1} for photodegradation of RhB, MB and MO (Fig. 6c), respectively. The results suggested that higher photocatalytic degradation ability was achieved for RhB compared to MO and MB, which was similar to the report by Yang et al. (2013).

To compare the photocatalytic activities of CdS with CdS/RGO nanocomposite towards degradation of RhB more efficiently, the apparent rate constant (*K*) was determined based on the pseudo-first-order reaction (Wu et al. 2015). The apparent rate constants
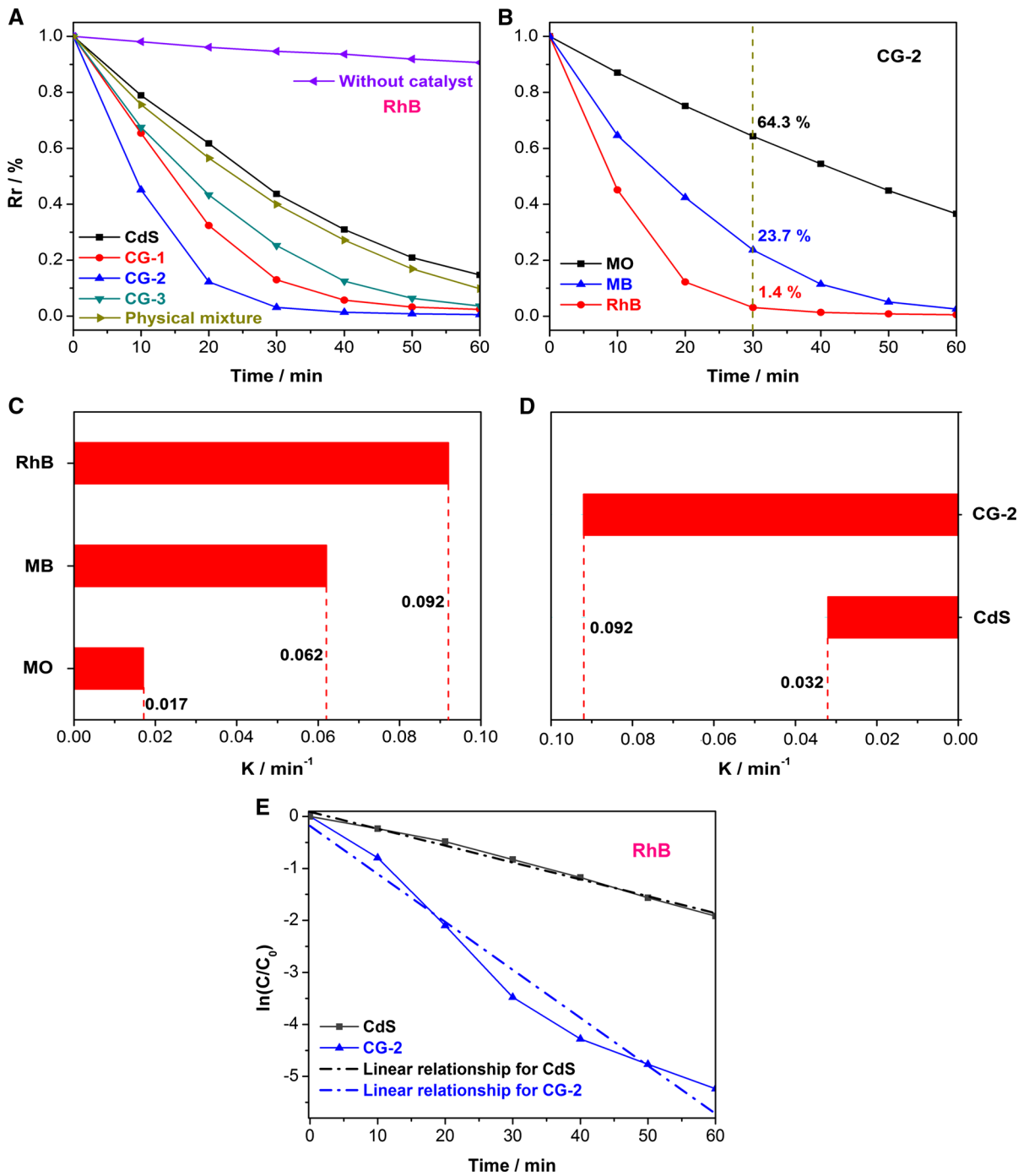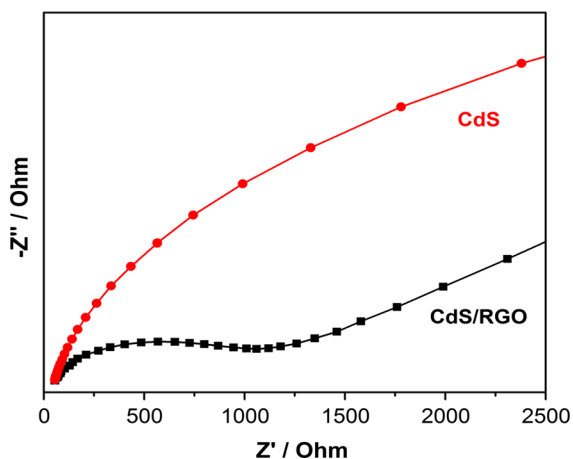
Fig. 6 **a** Photodegradation behaviors of RhB with CdS, CG-1, CG-2, CG-3 and physical mixture of CdS/GO; **b** photodegradation behaviors of RhB, MB and MO with CG-2; **c** the apparent rate constants of RhB, MB and MO on CG-2 as described in (**b**); **d** the apparent rate constants of RhB on CG-2 and CdS as described in (**a**); **e** the linear relationships of CdS and CG-2 for RhB degradation

were calculated as 3.2×10^{-2} and $9.2 \times 10^{-2} \, \text{min}^{-1}$ for CdS and CG-2 (Fig. 6d; the corresponding linear relationships of CdS and CG-2 for RhB degradation are displayed in Fig. 6e), respectively. The photocatalytic ability of CG-2 was almost 3 times higher than that of pure CdS (Fig. 6d). However, the CG-3 sample with the highest content of RGO showed the lowest activity for RhB degradation among all

nanocomposites synthesized by reflux condensation method, which was consistent with Zhang et al.'s report (2013c).

The EIS Nyquist plots (Bai et al. 2014), a strong tool in detecting the charge transfer process, were adopted to illuminate the performance advantage of CdS/RGO nanocomposite over CdS. Figure 7 depicts the result spectrum of EIS, indicating that the impedance arc radius of the CdS/RGO nanocomposite in the high-frequency region was smaller than that of pure CdS, which suggested improved conductive capability of CdS/RGO nanocomposite as compared with CdS (Zhang et al. 2009). These consequences were reasonable because RGO has a superior capability of capturing, storing, and transporting electrons through its sp^2 aromatic network (Zhang et al. 2012). Thus, when coupled with RGO, likelihood of the recombination of photoexcited electron–hole pairs from neat CdS could be greatly decreased, which eventually led to the higher photocatalytic activity of CdS/RGO nanocomposite over CdS.

According to those discussion and results, a mechanism of the improvement of photocatalytic activity of CdS anchored on RGO under solar irradiation was suggested and shown in Scheme 2. When CdS

Fig. 7 EIS spectrum of CdS and CdS/RGO nanocomposite

Scheme 2 The mechanism for dye degradation with CdS/RGO nanocomposite
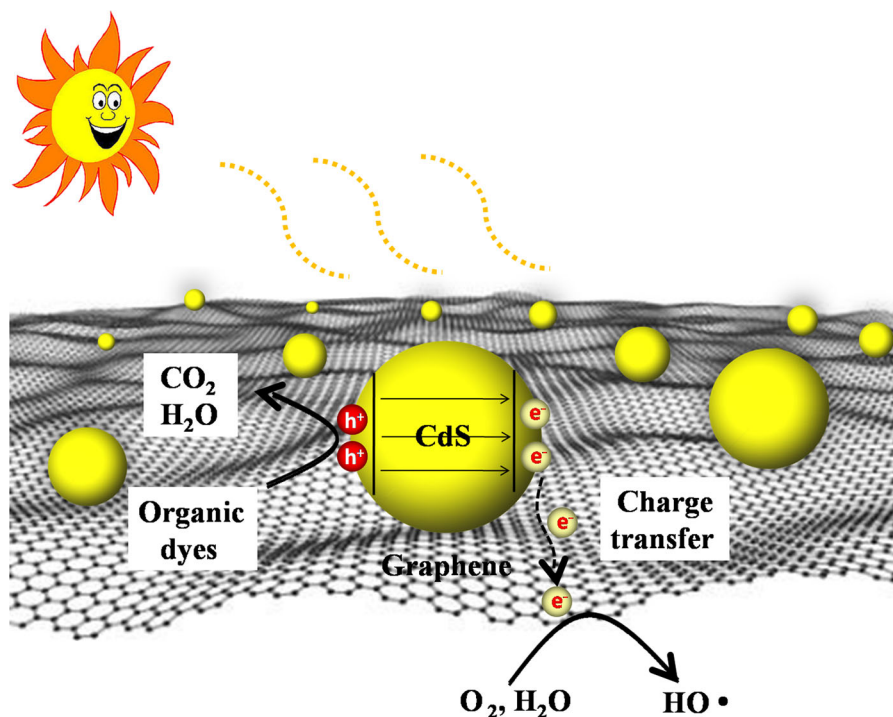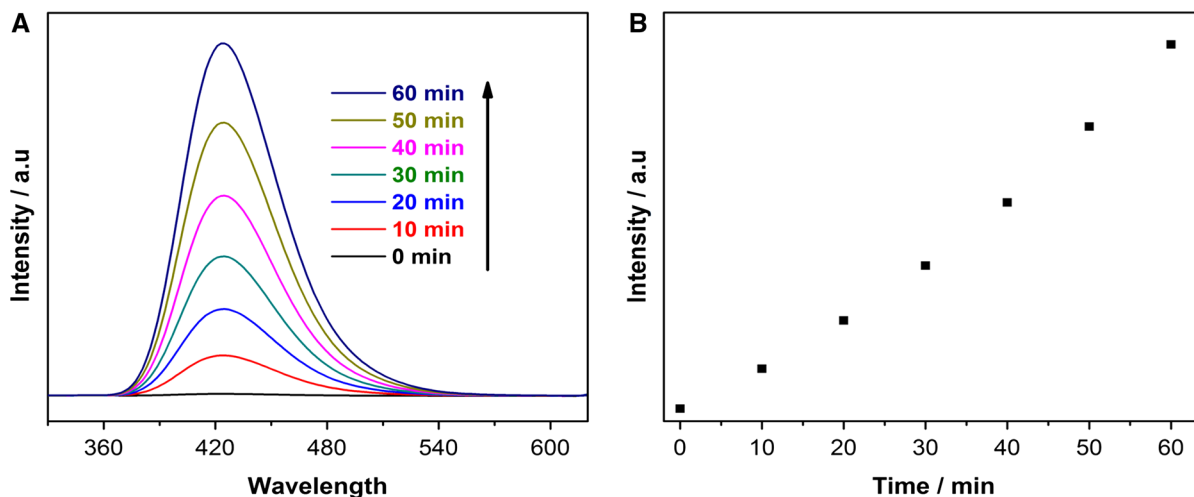
Fig. 8 a FL spectral changes observed during illumination of CdS/RGO nanocomposite under solar illumination; **b** FL intensity at 425 nm vs. illumination time for TAOH

deposited onto RGO nanosheets, an efficient nanointerface interaction between CdS and RGO was formed. The RGO nanosheets acted as a photogenerated charge transporter, which improved the charge transfer and reduced the recombination of electron–hole pairs of CdS (Chang et al. 2014). The separated electrons on the RGO surface further combined with adsorbed O_2 and H_2O to produce an OH· radical (Hoffmann et al. 1995), simultaneously, leaving holes in the valence band (VB) of CdS. However, the holes in VB of CdS could not oxidize OH^- to produce OH· radical because the VB potential of CdS (1.9 eV vs. NHE) is more negative than the redox potential of OH^-/·OH (2.7 eV vs. NHE) (Xiang et al. 2011). As known, holes and OH· possess powerful oxidative capacity and are in favor of destroying organic contaminants (Tanveer et al. 2014).

To demonstrate the presence of hydroxyl radicals (·OH), the fluorescence technique (FL) had been adopted. Terephthalic acid (TA) could react with reactive ·OH radicals and produced 2-hydroxy terephthalic acid (TAOH). TAOH could be excited at excitation wavelength of 315 nm and the maximum fluorescence intensity at 425 nm could be obtained (Chen et al. 2015b; Yi et al. 2015). The stronger the fluorescence intensity of TAOH was, more the OH· radicals were. As shown in Fig. 8a, with increasing irradiation time, fluorescence intensity increased. This result verified that the OH· radical was definitely produced under the solar radiation and Fig. 8b depicts that the FL intensity at 425 nm increased with irradiation time.

Conclusions

In summary, a reflux condensation method in water–DMF mixed solution for the synthesis of CdS/RGO nanocomposite was reported and the as-prepared CdS/RGO nanocomposite exhibited excellent photocatalytic activity for RhB degradation. The strong interface interaction, the strength of electron-vibration coupling and high light harvesting efficiency devoted to high photocatalytic activity of CdS/RGO nanocomposite, which demonstrated the efficiency construction approach. Furthermore, EIS technique verified that RGO could function as an excellent electron acceptor and transporter and the oxidizing hydroxyl radicals were also detected via FL spectrum. In addition, the results confirmed that the conductivity played an important role in the photocatalytic ability of CdS/RGO nanocomposite and the optimum content of RGO to CdS was 5 %. The advantages of this method for the synthesis of CdS/RGO nanocomposite lay in simple devices, utilization of common solvent and permitted large-scale production at low cost, which could pave the way for its wide application in reality.

References

Ai KL, Liu YL, Lu LH, Cheng XL, Huo LH (2011) A novel strategy for making soluble reduced graphene oxide sheets cheaply by adopting an endogenous reducing agent. J Mater Chem 21:3365–3370. doi:10.1039/C0JM02865G

Ajmal A, Majeed I, Malik RN, Idriss H, Nadeem MA (2014) Principles and mechanisms of photocatalytic dye degradation on TiO₂ based photocatalysts: a comparative overview. RSC Adv 4:37003–37026. doi:10.1039/C4RA06658H

Bai X, Zhang XY, Hua ZL, Ma WQ, Dai ZY, Huang X, Gu HX (2014) Uniformly distributed anatase TiO₂ nanoparticles on graphene: synthesis, characterization, and photocatalytic application. J Alloy Compd 599:10–18. doi:10.1016/j.jallcom.2014.02.049

Bera R, Kundu S, Patra A (2015) 2D Hybrid nanostructure of reduced graphene oxide-CdS nanosheet for enhanced photocatalysis. ACS Appl Mater Inter 7:13251–13259. doi:10.1021/acsami.5b03800

Cao AN, Liu Z, Chu SS, Wu MH, Ye ZM, Cai ZW, Chang YL, Wang SF, Gong QH, Liu YF (2010) A facile one-step method to produce graphene-CdS quantum dot nanocomposites as promising optoelectronic materials. Adv Mater 22:103–106. doi:10.1002/adma.200901920

Chang K, Mei ZW, Wang T, Kang Q, Ouyang SX, Ye JH (2014) MoS₂/graphene cocatalyst for efficient photocatalytic H₂ evolution under visible light irradiation. ACS Nano 8:7078–7087. doi:10.1021/nn5019945

Chen JZ, Wu XJ, Yin LS, Li B, Hong X, Fan ZX, Chen B, Xue C, Zhang H (2015a) One-pot synthesis of CdS nanocrystals hybridized with single-layer transition-metal dichalcogenide nanosheets for efficient photocatalytic hydrogen evolution. Angew Chem 127:1226–1230. doi:10.1002/anie.201410172

Chen XF, Dai JF, Shi GF, Li L, Wang GY, Yang H (2015b) Visible light photocatalytic degradation of dyes By β-Bi₂O₃/graphene nanocomposites. J Alloy Compd 649:872–877. doi:10.1016/j.jallcom.2015.05.096

Deng CH, Ge XQ, Hu HM, Yao L, Han CL, Zhao DF (2014) Template-free and green sonochemical synthesis of hierarchically structured CuS hollow microspheres displaying excellent Fenton-like catalytic activities. CrystEngComm 16:2738–2745. doi:10.1039/C3CE42376J

Etmimi HM, Sanderson RD (2011) New approach to the synthesis of exfoliated polymer/graphite nanocomposites by miniemulsion polymerization using functionalized graphene. Macromolecules 44:8504–8515. doi:10.1021/ma2003008

Gao P, Liu JC, Sun DD, Ng W (2013) Graphene oxide-CdS composite with high photocatalytic degradation and disinfection activities under visible light irradiation. J Hazard Mater 250:412–420. doi:10.1016/j.jhazmat.2013.02.003

Ge L, Zuo F, Liu JK, Ma Q, Wang C, Sun DZ, Bartels L, Feng PY (2012) Synthesis and efficient visible light photocatalytic hydrogen evolution of polymeric g-C₃N₄ coupled with CdS quantum dots. J Phys Chem C 116:13708–13714. doi:10.1021/jp3041692

Guo JS, Zhang T, Hu CG, Fu L (2015) A three-dimensional nitrogen-doped graphene structure: a highly efficient carrier of enzymes for biosensors. Nanoscale 7:1290–1295. doi:10.1039/C4NR05325G

Han SC, Hu LF, Gao N, Al-Ghamdi AA, Fang XS (2015) Efficient self-assembly synthesis of uniform CdS spherical nanoparticles-Au nanoparticles hybrids with enhanced photoactivity. Adv Funct Mater 24:3725–3733. doi:10.1002/adfm.201400012

Hoffmann MR, Martin ST, Choi WY, Bahnemann DW (1995) Environmental applications of semiconductor photocatalysis. Chem Rev 95:69–96. doi:10.1021/cr00033a004

Kaveri S, Thirugnanam L, Dutta M, Ramasamy J, Fukata N (2013) Thiourea assisted one-pot easy synthesis of CdS/rGO composite by the wet chemical method: structural, optical, and photocatalytic properties. Ceram Int 39:9207–9214. doi:10.1016/j.ceramint.2013.05.025

Konstantinou IK, Albanis TA (2004) TiO₂-assisted photocatalytic degradation of azo dyes in aqueous solution: kinetic and mechanistic investigations: a review. Appl Catal B-Environ 49:1–14. doi:10.1016/j.apcatb.2003.11.010

Li Q, Guo BD, Yu JG, Ran JR, Zhang BH, Yan HJ, Gong JR (2011) Highly efficient visible-light-driven photocatalytic hydrogen production of CdS-cluster-decorated graphene nanosheets. J Am Chem Soc 133:10878–10884. doi:10.1021/ja2025454

Li Q, Li X, Wageh S, Al-Ghamdi AA, Yu JG (2015a) CdS/Graphene nanocomposite photocatalysts. Adv Energy Mater 5. doi:10.1002/aenm.201500010

Li SG, Zhu W, Xue YC, Liu SQ (2015b) Construction of photoelectrochemical thrombin aptasensor via assembling multilayer of graphene-CdS nanocomposites. Biosens Bioelectron 64:611–617. doi:10.1016/j.bios.2014.09.072

Liu XJ, Pan LK, Lv T, Zhu G, Sun Z, Sun CQ (2011) Microwave-assisted synthesis of CdS-reduced graphene oxide composites for photocatalytic reduction of Cr(VI). Chem Commun 47:11984–11986. doi:10.1039/C1CC14875C

Liu SQ, Chen Z, Zhang N, Tang ZR, Xu YJ (2013) An efficient self-assembly of CdS nanowires-reduced graphene oxide nanocomposites for selective reduction of nitro organics under visible light irradiation. J Phys Chem C 117:8251–8261. doi:10.1021/jp400550t

Liu H, Lv T, Wu XH, Zhu CK, Zhu ZF (2014) Preparation and enhanced photocatalytic activity of CdS@ RGO core-shell structural microspheres. Appl Surf Sci 305:242–246. doi:10.1016/j.apsusc.2014.03.045

Liu XY, Zhou YF, Nie WY, Song LY, Chen PP (2015) Fabrication of hydrogel of hydroxypropyl cellulose (HPC) composited with graphene oxide and its application for methylene blue removal. J Mater Sci 50:6113–6123. doi:10.1007/s10853-015-9166-y

Meng NN, Zhang SJ, Zhou YF, Nie WY, Chen PP (2015a) Novel synthesis of silver/reduced graphene oxide nanocomposite and its high catalytic activity towards hydrogenation of 4-nitrophenol. RSC Adv 5:70968–70971. doi:10.1039/C5RA13574E

Meng NN, Zhou YF, Nie WY, Song LY, Chen PP (2015b) CuS/MoS$_2$ nanocomposite with high solar photocatalytic activity. J Nanopart Res 17:1–10. doi:10.1007/s11051-015-3105-3

Nethravathi C, Nisha T, Ravishankar N, Shivakumara C, Rajamathi M (2009) Graphene-nanocrystalline metal sulphide composites produced by a one-pot reaction starting from graphite oxide. Carbon 47:2054–2059. doi:10.1016/j.carbon.2009.03.055

Paramasivam I, Jha H, Liu N, Schmuki P (2012) A review of photocatalysis using self-organized TiO$_2$ nanotubes and other ordered oxide nanostructures. Small 8:3073–3103. doi:10.1002/smll.201200564

Park J, Park S, Selvaraj R, Kim Y (2015) Microwave-assisted synthesis of Au/CdS nanorods for a visible-light responsive photocatalyst. RSC Adv 5:52737–52742. doi:10.1039/C5RA07620J

Qu Y, Duan X (2013) Progress, challenge and perspective of heterogeneous photocatalysts. Chem Soc Rev 42:2568–2580. doi:10.1039/c2cs35355e

Shown I, Hsu HC, Chang YC, Lin CH, Roy PK, Ganguly A, Wang CH, Chang JK, Wu CI, Chen LC (2014) Highly efficient visible light photocatalytic reduction of CO$_2$ to hydrocarbon fuels by Cu-nanoparticle decorated graphene oxide. Nano Lett 14:6097–6103. doi:10.1021/nl503609v

Singh V, Joung D, Zhai L, Das S, Khondaker SI, Seal S (2011) Graphene based materials: past, present and future. Prog Mater Sci 56:1178–1271. doi:10.1016/j.pmatsci.2011.03.003

Song SY, Gao W, Wang X, Li XY, Liu DP, Xing Y, Zhang HJ (2012) Microwave-assisted synthesis of BiOBr/graphene nanocomposites and their enhanced photocatalytic activity. Dalton Trans 41:10472–10476. doi:10.1039/C2DT31088K

Tanveer M, Cao CB, Ali Z, Aslam I, Idrees F, Khan WS, But FK, Tahir M, Mahmood N (2014) Template free synthesis of CuS nanosheet-based hierarchical microspheres: an efficient natural light driven photocatalyst. CrystEngComm 16:5290–5300. doi:10.1039/C4CE00090K

Veamatahau A, Jiang B, Seifert T, Makuta S, Latham K, Kanehara M, Teranishi T, Tachibana Y (2015) Origin of surface trap states in CdS quantum dots: relationship between size dependent photoluminescence and sulfur vacancy trap states. Phys Chem Chem Phys 17:2850–2858. doi:10.1039/C4CP04761C

Wu LH, Zhou YF, Nie WY, Song LY, Chen PP (2015) Synthesis of highly monodispersed teardrop-shaped core-shell SiO$_2$/TiO$_2$ nanoparticles and their photocatalytic activities. Appl Surf Sci 351:320–326. doi:10.1016/j.apsusc.2015.05.152

Xiang QJ, Yu JG, Wong PK (2011) Quantitative characterization of hydroxyl radicals produced by various photocatalysts. J Colloid Interf Sci 357:163–167. doi:10.1016/j.jcis.2011.01.093

Xiao FX, Miao JW, Liu B (2014) Layer-by-layer self-assembly of CdS quantum dots graphene nanosheets hybrid films for photoelectrochemical and photocatalytic applications. J Am Chem Soc 136:1559–1569. doi:10.1021/ja411651e

Yan JF, Ye Q, Wang XL, Yu B, Zhou F (2012) CdS/CdSe quantum dot co-sensitized graphene nanocomposites via polymer brush templated synthesis for potential photovoltaic applications. Nanoscale 4:2109–2116. doi:10.1039/C2NR11893A

Yang XF, Cui HY, Li Y, Qin JL, Zhang RX, Tang H (2013) Fabrication of Ag$_3$PO$_4$-graphene composites with highly efficient and stable visible light photocatalytic performance. ACS Catal 3:363–369. doi:10.1021/cs3008126

Yi SS, Zhao F, Yue XZ, Wang DJ, Lin YH (2015) Enhanced solar light-driven photocatalytic activity of BiOBr-ZnO heterojunctions with effective separation and transfer properties of photo-generated chargers. New J Chem 39:6659–6666. doi:10.1039/C5NJ00707K

Yin ZY, Zhu JX, He QY, Cao XH, Tan CL, Chen HY, Yan QY, Zhang H (2014) Graphene-based materials for solar cell applications. Adv Energy Mater 4. doi:10.1002/aenm.201300574

Yu JG, Jin J, Cheng B, Jaroniec M (2014) A noble metal-free reduced graphene oxide-CdS nanorod composite for the enhanced visible-light photocatalytic reduction of CO$_2$ to solar fuel. J Mater Chem A 2:3407–3416. doi:10.1039/C3TA14493C

Yuan K, Chen L, Tan LC, Chen YW (2014) Performance enhancement of bulk heterojunction solar cells with direct growth of CdS-cluster-decorated graphene nanosheets. Chem Eur J 20:6010–6018. doi:10.1002/chem.201400119

Zhang H, Lv XJ, Li YM, Wang Y, Li JH (2009) P25-graphene composite as a high performance photocatalyst. ACS Nano 4:380–386. doi:10.1021/nn901221k

Zhang JL, Yang HJ, Shen GX, Cheng P, Zhang JY, Guo SW (2010) Reduction of graphene oxide via L-ascorbic acid. Chem Commun 46:1112–1114. doi:10.1039/B917705A

Zhang XT, Sui ZY, Xu B, Yue SF, Luo YJ, Zhan WC, Liu B (2011) Mechanically strong and highly conductive graphene aerogel and its use as electrodes for electrochemical power sources. J Mater Chem 21:6494–6497. doi:10.1039/C1JM10239G

Zhang N, Zhang YH, Pan XY, Yang MQ, Xu YJ (2012) Constructing ternary CdS-graphene-TiO$_2$ hybrids on the flatland of graphene oxide with enhanced visible-light photoactivity for selective transformation. J Phys Chem C 116:18023–18031. doi:10.1021/jp303503c

Zhang N, Yang MQ, Tang ZR, Xu XJ (2013a) Toward improving the graphene-semiconductor composite photoactivity via the addition of metal ions as generic interfacial mediator. ACS Nano 8:623–633. doi:10.1021/nn405242t

Zhang N, Zhang YH, Yang MQ, Tang ZR, Xu YJ (2013b) A critical and benchmark comparison on graphene-, carbon nanotube-, and fullerene-semiconductor nanocomposites as visible light photocatalysts for selective oxidation. J Catal 299:210–221. doi:10.1016/j.jcat.2012.11.021

Zhang YY, Tang YX, Liu XF, Dong ZL, Hng HH, Chen Z, Sum TC, Chen XD (2013c) Three-dimensional CdS-titanate composite nanomaterials for enhanced visible-light-driven hydrogen evolution. Small 9:996–1002. doi:10.1002/smll.201202156

Zhao D, Sheng G, Chen C et al (2012) Enhanced photocatalytic degradation of methylene blue under visible irradiation on graphene@TiO$_2$ dyade structure. Appl Catal B Environ 111:303–308. doi:10.1016/j.apcatb.2011.10.012